PAPER • OPEN ACCESS

UV-Vis spectroscopic and colorimetric anion detection and fluorescence properties of new 3-amino-4-hydroxybenzenesulfonic acid-based Schiff bases depending on the strength and position of the electron donor substitution

To cite this article: Elif Akhuseyin Yildiz *et al* 2023 *Phys. Scr.* **98** 085409

View the article online for updates and enhancements.

You may also like

- Voltammetry of 4-Hydroxybiphenyl
Inam U. Haque, Ashi Rashid and Muqaddas Tariq
- Preparation and characterization of poly(3-hydroxybutyrate-co-4-hydroxybutyrate)/pullulan-gelatin electrospun nanofibers with shell-core structure
Fanchen Sun, Jing Guo, Yuanfa Liu et al.
- Synthesis, docking molecule study and antibacterial activity of N'-(4-Fluorobenzylidene)-4-hydroxybenzohydrazide and N'-(4-Fluorobenzylidene)-4-hydroxybenzohydrazide)
S Suzana, M I Sulistyowaty, Isnaeni et al.

This content was downloaded from IP address 80.251.45.167 on 21/08/2023 at 22:39

Physica Scripta

PAPER

UV-Vis spectroscopic and colorimetric anion detection and fluorescence properties of new 3-amino-4-hydroxybenzenesulfonic acid-based Schiff bases depending on the strength and position of the electron donor substitution

Elif Akhuseyin Yildiz[1,*], **Yasemin Pepe**[1], **Diğdem Erdener**[2], **Ahmet Karatay**[1], **Bahadir Boyacioglu**[3,*], **Hüseyin Ünver**[4], **Gönül Yapar**[5], **Neslihan Demir**[6], **Mustafa Yıldız**[2,*] and **Ayhan Elmali**[1]

[1] Department of Physics Engineering, Faculty of Engineering, Ankara University, 06100 Beşevler-Ankara, Turkey
[2] Department of Chemistry, Faculty of Sciences, Çanakkale Onsekiz Mart University, 17100 Çanakkale, Turkey
[3] Vocational School of Health Services, Ankara University, 06290 Kecioren-Ankara, Turkey
[4] Department of Physics, Faculty of Science, Ankara University, 06100 Besevler-Ankara, Turkey
[5] Department of Chemistry, Faculty of Arts and Sciences, Istanbul Technical University, Istanbul, Turkey
[6] Department of Biology, Faculty of Sciences, Çanakkale Onsekiz Mart University, 17100 Çanakkale, Turkey
[*] Authors to whom any correspondence should be addressed.

E-mail: eakhuseyin@ankara.edu.tr, bboyacioglu@ankara.edu.tr and myildiz@comu.edu.tr

OPEN ACCESS

RECEIVED
1 March 2023

REVISED
5 July 2023

ACCEPTED FOR PUBLICATION
17 July 2023

PUBLISHED
31 July 2023

Original content from this work may be used under the terms of the Creative Commons Attribution 4.0 licence.

Any further distribution of this work must maintain attribution to the author(s) and the title of the work, journal citation and DOI.

Keywords: biological activity, 3-amino-4-hydroxybenzenesulfonic acid, femtosecond transient absorption spectroscopy, anion sensor, DPPH method, density functional theory (DFT)

Supplementary material for this article is available online

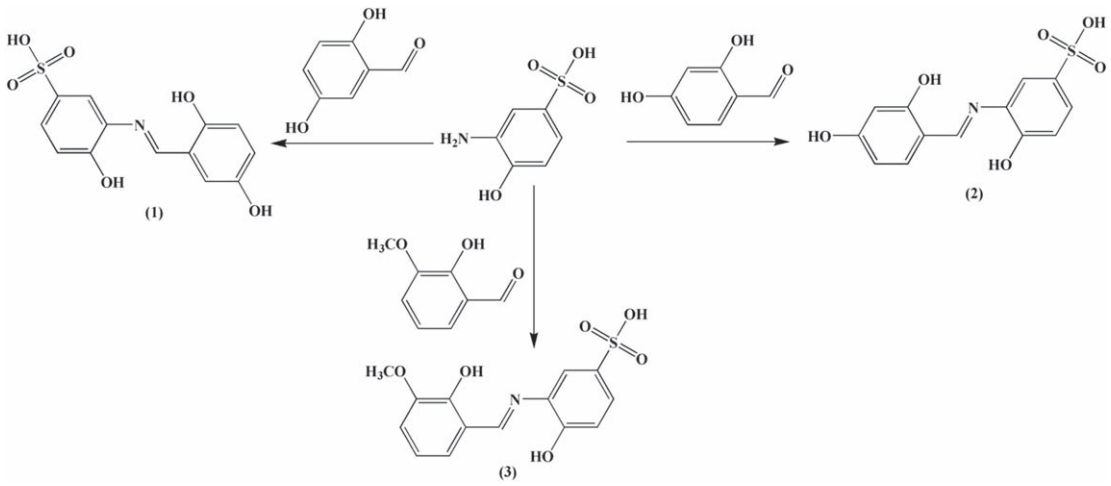
Abstract

In this study, 3-amino-4-hydroxybenzenesulfonic acid-based imine compounds; 3-(2,5-dihydroxybenzylideneamino)-4-hydroxybenzenesulfonic acid (**1**), 3-(2,4-dihydroxybenzylideneamino)-4-hydroxybenzenesulfonic acid (**2**) and 4-hydroxy-3-(2-hydroxy-3-methoxybenzylideneamino)-4-hydroxybenzenesulfonic acid (**3**) was synthesized. The compounds were analyzed using various spectroscopy methods, and the experimental UV–vis data matched the theoretical predictions. The compound **1** displayed lower stability, higher reactivity, and easier photoexcitation due to a smaller HOMO-LUMO energy gap. The investigated compounds **1-3** showed promise as chemosensors for anions, providing visible detection in daylight conditions. The compound **3** exhibited selective fluorescence at specific wavelengths. The compounds **1-3** interacted with DNA through electrostatic interactions. Also, compounds **1-3** showed higher antioxidant activity than BHT. However, fluorescence measurements indicated that the emission signals were strongly influenced by the position and strength of the electron-donating group. Adding a hydroxy or methoxy moiety near the -OH group on the phenyl ring decreased the fluorescence signal due to intersystem crossing and intramolecular charge transfer mechanisms, respectively. These findings were supported by femtosecond transient absorption spectroscopy measurements. The results emphasize the significance of substituents in imines derived from 3-amino-4-hydroxybenzenesulfonic acid in determining their biological activities, as well as their optical and sensor properties.

1. Introduction

Schiff bases are important organic synthetic reagents and liquid crystal materials in chemistry, and their significance has increased recently [1]. These compounds are generated through the condensation reaction between primary amines and carbonyl compounds [2]. The synthesis of new amines and carbonyl compounds has led to the discovery of many new types of Schiff bases, expanding their properties and application areas [1–3]. Schiff bases, particularly those with chelating properties, have found applications as auxiliary pharmacophores in the production of bioactive lead compounds, as well as in various biological applications [4].

© 2023 The Author(s). Published by IOP Publishing Ltd



Scheme 1. Synthesis of compounds 1–3.

They exhibit antifungal and antibacterial activities, and their metal complexes have been studied for potential anticancer and herbicide applications, making them valuable models for biologically significant species. Ongoing research explores their antibacterial, antifungal, antiviral, antitumor, anti-inflammatory, anti-HIV, and anticancer properties [5–16]. The complexes formed by these compounds often exhibit higher antimicrobial efficacy compared to their individual ligands [5, 9, 16, 17].

In the field of optical properties, studies have been conducted on quinoline-derived imines and the use of ZnO nanoparticles for laser applications [18]. Schiff base ZnO complexes have been investigated as potential semiconductors, and fluorescent probes based on oxo-spirocyclic bridging Schiff bases have shown sensitive and selective responses to zinc(II) ions [19, 20]. Some Schiff base metal complexes with accessible band gaps have been explored as conductive/semiconductor materials [21]. Additionally, the fluorescence properties and thin-layer applications of optically active Schiff bases and their Ag(I) complexes have been investigated, revealing interesting photoluminescent properties [22].

In recent years, there has been a focus on synthesizing and developing new molecules for detecting harmful chemical species in the environment. Schiff-based fluorescence sensors have gained popularity due to their high sensitivity, particularly at low analyte concentrations. These chemosensors exhibit great selectivity and sensitivity for sensing ions and can induce noticeable changes in color and absorption spectra, making them preferred options for ion-selective sensing. Schiff bases display phenol-imine↔keto-amine tautomerism, which is attributed to intramolecular proton transfer and donor-acceptor behavior. Many of their properties can be explained through their tautomeric forms. These compounds find applications in various scientific fields and industrial sectors, and further research is needed to explore their biological activity and technological applications. Schiff bases hold promise for the design and development of more effective biological, optical, industrial, and chromogenic agents, necessitating a deeper understanding of their mechanisms and structure-activity relationships [23–30].

In the presented work, a new class of imine compounds was synthesized by reacting 3-amino-4-hydroxybenzenesulfonic acid with 2-hydroxybenzaldehyde containing an electron-donating group (Scheme 1). The aim was to investigate the mechanism of their sensor behaviors. The synthesized compounds were evaluated for their ability to sense anions using spectroscopic and calorimetric methods. Additionally, their antimicrobial effects, interactions with DNA (including binding and cleavage abilities), and antioxidant properties were examined. The emission spectra of the compounds were tracked, and ultrafast pump-probe spectroscopy measurements were used to study charge transfer dynamics and decay kinetics. The electronic and optical characteristics of the compounds were analyzed using density functional theory (DFT). This work opens up new possibilities for designing acid-based Schiff bases for biological activity and anion sensing, utilizing various common Schiff bases with organosulfur components.

2. Materials and methods

2.1. Reagents and techniques

NMR spectra of the compounds were acquired using a Bruker AVANCE-500 spectrometer operating at 400 and 101.6 MHz in DMSO. FT-IR spectra were obtained using a Perkin Elmer BX II spectrometer, with KBr discs

serving as the sample medium. UV–vis spectra were measured using a SHIMADZU 1800 series spectrophotometer. MS analysis was recorded with a SHIMADZU LCMS-8040 triple quadrupole mass spectrometer. Melting points were determined using an Electro-Thermal IA 9100 instrument, employing a capillary tube. Elemental analysis was conducted using a Vario EL III CHNS elemental analyzer. 3-Amino-4-hydroxybenzenesulfonic acid, 2,5-dihydroxybenzaldehyde, 2,4-dihydroxybenzaldehyde, 2-hydroxy-3-methoxybenzaldehyde, ethidium bromide (EB, powder), calf thymus DNA (CT-DNA), pBR322 DNA, 2,2-diphenyl-1-picrylhydrazyl (DPPH), butylated hydroxytoluene (BHT), $(Bu)_4NF$, $(Bu)_4NBr$, $(Bu)_4NI$, $(Bu)_4NCN$, $(Bu)_4NSCN$, $(Bu)_4NClO_4$, $(Bu)_4NHSO_4$, $(Bu)_4NCH_3COO$, $(Bu)_4NH_2PO_4$, $(Bu)_4NN_3$, $(Bu)_4NOH$, EtOH, $CHCl_3$, n-Hexane and dimethyl sulfoxide (DMSO) were purchased from Aldrich. All chemicals were used as received.

2.2. Synthesis

2.2.1. Synthesis of 3-(2,5-dihydroxybenzylideneamino)-4-hydroxybenzenesulfonic acid (Compound 1)

3-Amino-4-hydroxybenzenesulfonic acid (0.95 g, 5.0×10^{-3} mol) was added to EtOH (100 ml) solution of 2,5-dihydroxybenzaldehyde (0.69 g, 5.0×10^{-3} mol). The mixture was stirred and refluxed for 2 h. Compound 1 was obtained from the evaporation of EtOH. The crude product was purified from $CHCl_3$:n-hexane (3:2) as a pale green solid, m.p > 300 °C, 1.13 g (73%) yield. Found: C, 50.45; H, 3.59; N, 4.53. Calc. For $C_{13}H_{11}NO_6S$; C, 50.48; H, 3.55; N, 4.53%. FT-IR (KBr, cm^{-1}, figure S1; Supplementary); νO-H; 3841-3736-3613-3538-3449 s-br, νAr-H; 3243–3103 s-br, νC–H; 2927–2865 s, νC=N; 1739 s, νC=C; 1645–1561–1513 s, νC–N; 1452 s, νC-O; 1397 s. ^{1}H-NMR (DMSO, figure S2); δ ppm, 10.88 (s, 1H, Ar–O<u>H</u>); 10.18 (s, 1H, Ar-O<u>H</u>); 9.80 (br, 1H, Ar-O<u>H</u>); 9.34 (s, 1H, Ar-C<u>H</u>=N-); 7.94–6.83 (m, 6H, Ar-<u>H</u>), 4.10 (s-br, 1H, SO_2-O<u>H</u>). ^{13}C–NMR (DMSO, figure S3); δ ppm, 191.71 (s, C7), 162.05(s, C9), 154.40(s, C6), 151.31(s, C3), 150.45(s, C12), 140.50(s, C8), 127.35(s, C11), 124.99(s, C13), 122.74(s, C1), 122.36(s, C4), 118.93(s, C10), 115.60(s, C5), 113.12(s, C2).

2.2.2. Synthesis of 3-(2,4-dihydroxybenzylideneamino)-4-hydroxybenzenesulfonic acid (Compound 2)

3-Amino-4-hydroxybenzenesulfonic acid (0.95 g, 5.0×10^{-3} mol) was added to EtOH (100 ml) solution of 2,4-dihydroxybenzaldehyde (0.69 g, 5.0×10^{-3} mol). The mixture was stirred and refluxed for 2 h. Compound 2 was obtained from the evaporation of EtOH. The crude product was purified from $CHCl_3$:n-hexane (3:2) as a yellow solid, m.p > 300 °C, 1.15 g (74%) yield. Found: C, 50.46; H, 3.60; N, 4.53. Calc. For $C_{13}H_{11}NO_6S$; C, 50.48; H, 3.55; N, 4.53%. FT-IR (KBr, cm^{-1}, figure S1; Supplementary); νO–H; 3863-3740-3516-3401 s-br, νAr-H; 3261 s-br, νC–H; 2962 s, νC=N; 1739 s, νC=C; 1644-1599-1539 s, νC-N; 1449 s, νC-O; 1397 s. ^{1}H-NMR (DMSO, figure S4); δ ppm, 11.24 (s, 1H, Ar-O<u>H</u>); 10.89 (s, 1H, Ar-O<u>H</u>); 9.92 (s, 1H, Ar-O<u>H</u>); 9.39 (s, 1H, Ar-C<u>H</u>=N-); 8.04–6.32 (m, 6H, Ar–<u>H</u>), 3.90 (s-br, 1H, SO_2-O<u>H</u>). ^{13}C–NMR (DMSO, figure S5); δ ppm, 191.34 (s, C7), 168.88(s, C6), 165.16(s, C4), 159.47(s, C9), 149.42(s, C12), 141.34(s, C8), 133.20(s, C2), 127.59(s, C11), 124.86(s, C13), 118.16(s, C10), 111.35(s, C1), 109.08(s, C3), 102.93(s, C5).

2.2.3. Synthesis of 4-hydroxy-3-(2-hydroxy-3-methoxybenzylideneamino)-4-hydroxy benzenesulfonic acid (Compound 3)

3-Amino-4-hydroxybenzenesulfonic acid (0.95 g, 5.0×10^{-3} mol) was added to EtOH (100 ml) solution of 2-hydroxy-3-methoxybenzaldehyde (0.76 g, 5.0×10^{-3} mol). The mixture was stirred and refluxed for 2 h. Compound 3 was obtained from the evaporation of EtOH. The crude product was purified from CHCl3:n-hexane (3:2) as a yellowish-brown solid, m.p > 300 °C, 1.13 g (70%) yield. Found: C, 52.03; H, 4.03; N, 4.33. Calc. For $C_{14}H_{13}NO_6S$; C, 52.01; H, 4.02; N, 4.33%. FT-IR (KBr, cm^{-1}, figure S1; Supplementary); νO-H; 3850-3745-3402-3353 s-br, νAr-H; 3287 s-br, νC–H; 2918–2861 s, νC=N; 1736 s, νC=C; 1643–1502 s, νC–N; 1458 s, νC–O; 1353 s, Ar–O–CH_3; 1289-1254-1182-1094 s-br. ^{1}H-NMR (DMSO, figure S6); δ ppm, 10.99 (s, 1H, Ar-O<u>H</u>); 10.27 (s, 1H, Ar–O<u>H</u>); 9.29 (s, 1H, Ar–O<u>H</u>); 8.96 (s, 1H, Ar–C<u>H</u>=N–); 7.83–6.89 (m, 6H, Ar-<u>H</u>), 4.05 (s-br, 1H, SO_2-O<u>H</u>); 3.85 (s, 3H, Ar-OC<u>H</u>$_3$). ^{13}C-NMR (DMSO, figure S7); δ ppm, 192.43 (s, C7), 162.27(s, C9), 151.17(s, C5), 148.82(s, C6), 140.51(s, C12), 127.36(s, C8), 125.48(s, C11), 122.98(s, C13), 122.37(s, C2), 120.54(s, C3), 119.67(s, C1), 118.05(s, C10), 115.60(s, C4), 56.56(s, C14).

2.3. Anion sensors measurements

The methods described in the references [28–31] were followed to prepare solutions of compounds 1–3, along with tetrabutylammonium salts, in DMSO at a concentration of 50 μM. These solutions were used for colorimetric and spectroscopic investigations.

2.4. Screening for antimicrobial activities

In this study, different microorganisms were utilized, including *Pseudomonas aeruginosa* ATCC 27853, *Escherichia coli* ATCC 25922, Proteus vulgaris ATCC 13315, Bacillus subtilis ATCC 6633, Saphylococcus aureus

Table 1. MIC and MBC values (μg/ml) of the title compound[a,b].

Microorganisms	Compound			Antibiotic gentamicin ampicillin fluconazole			MBC (1)	MBC (2)	MBC (3)
	(1)	(2)	(3)						
P. aeruginosa ATCC 27853	256	256	128	0.08	2		>1024	>1024	>1024
E. coli ATCC 25922	256	256	256	0.125	32		512	>1024	>1024
P. vulgaris ATCC 13315	256	256	128	0.125	0.06		512	512	512
B. Subtilis ATCC 6633	128	256	128	0.008	0.06	—	>1024	>1024	>1024
S. aureus ATCC 25923	128	128	64	1	0.016	—	>1024	>1024	>1024
E. faecalis ATCC 29212	32	128	64	1	0.016		>1024	>1024	>1024
C. albicans 60193	256	256	64	—	—	0.063	256	256	64
C. tropicalis ATCC 13803	16	16	—	—	—	0.5	16	16	>1024

[a] The minimum inhibitory concentration (MIC).

[b] The minimum bactericidal concentration (MBC).

ATCC 25923, Enterococcus faecalis ATCC 29212, *Candida albicans* ATCC 60193, and *Candida tropicalis* ATCC 13803. To make comparisons, control antibiotics such as gentamicin, ampicillin, and fluconasol were employed. The experimental setup followed the methodology described in reference [31]. The data presented in table 1 represent the average values obtained from three separate experiments.

2.5. DNA-Binding experiments

The methodology described in the references [31, 32] was followed to investigate the binding affinity of the compounds for DNA using UV–vis spectroscopy. This examination was conducted in the presence and absence of CT-DNA.

2.6. DNA-Cleavage experiments

The investigation evaluated the ability of the compound to induce DNA cleavage by employing gel electrophoresis. The procedure described in reference [31] was followed for this assessment. Supercoiled (SC) pBR322 DNA was used as the DNA substrate in this study.

2.7. Antioxidant activity (DPPH: UV–visible based assay)

Antioxidant activity studies were performed using the 1,1-Diphenyl-2-picrylhydrazyl radical (DPPH) method [33], and a comparison was made using the antioxidant butylated hydroxytoluene (BHT) standard [34]. The study was performed according to reference [31] with a UV–visible spectrophotometer to monitor the change in absorbance at 517 nm and then calculate the antioxidant activity of the compounds.

2.8. Theoretical method

The molecular geometries of these compounds were initially constructed using the Gaussview 5.0 visualization program [35]. Subsequently, we optimized the molecular structures of the compounds in their ground state using the DFT/B3LYP method and a 6–311++G(d,p) basis set [36, 37], employing the Gaussian 09 W software package [38]. Furthermore, we used TD-DFT/CAM-B3LYP with a 6–311++G(d,p) basis set to theoretically derive the maximum UV–vis absorption spectra. It should be noted that B3LYP is a valuable computational technique for modeling electronic properties of systems in their ground state, while CAM-B3LYP is better suited for matching optical properties with experimental data [39–41].

To evaluate the energies of the frontier molecular orbitals (HOMO and LUMO), the molecular electrostatic potential (MEP), and the energy gap between HOMO and LUMO, we employed the DFT approach with a B3LYP basis set, considering a DMSO solvent environment. Additionally, using the Multiwfn software [42], we analyzed the distribution of holes and electrons between the ground state (S0) and the first excited state (S1) excitation. These calculations can be compared with our previous work on the development and design of a sulfonamide-based Schiff base series [28–30].

2.9. Optical measurements

The steady-state absorption spectra of compounds 1–3 in DMSO were recorded using a Shimadzu UV-1800 scanning spectrophotometer. For fluorescence spectral measurements, a Perkin Elmer LS55 spectrophotometer was employed. To conduct femtosecond transient absorption spectroscopy measurements, a mode-locked Ti: Sapphire laser amplifier and an optical parametric amplifier system (Spectra-Physics, Spitfire Pro XP, TOPAS) were utilized. The laser system operated with a pulse duration of 52 fs and a repetition rate of 1 kHz. To study the

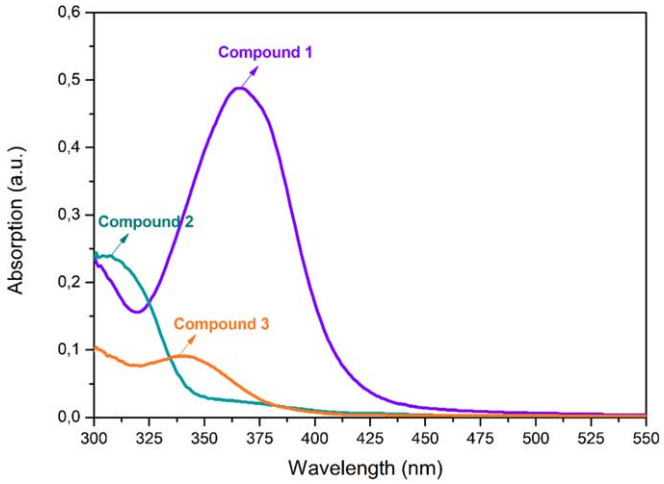


Figure 1. Absorption spectra of compounds 1–3 with 5×10^{-5} M in DMSO solution.

charge transfer dynamics and decay traces of compounds 1–3 in DMSO, a commercial pump-probe experimental setup (Spectra-Physics, Helios) was used. The probe light used was a white light continuum, while the pump wavelength was determined based on linear absorption spectra. The excited state dynamics were measured over a timescale ranging from 0.1 ps to 3.2 ns. Transient absorption data was collected using a fiber-coupled spectrometer connected to a computer. The femtosecond transient experimental data were analyzed using the Surface Xplorer software, supported by Ultrafast Systems.

3. Results and discussion

3.1. FTIR, MS, ^{1}H NMR, ^{13}C NMR and UV–vis spectra

FT-IR spectra of the compounds are given in figure S1 and all vibrations belonging to characteristic functional groups were observed. Characteristic C=N stretching vibrations for compounds 1, 2 and 3 were observed at 1739, 1739 and 1736 cm^{-1}. Since the methoxy group donates fewer electrons to the ring than the other OH groups, the vibration of the C=N bond in compound 3 occurred at a lower frequency. In addition, the fact that phenol-imin↔keto-amine tautomer was not observed in all (1–3) compounds according to UV–vis results strengthens this situation. The stretching vibrations owing to the Ar–O–CH_3 group were observed at 1289-1254-1182-1094 cm^{-1} for compound 3. For compounds 1–3, SO_2 vibrations were found in the ranges of 1208–1173, 1273-1173-1112 and 1284–1038 cm^{-1}, respectively [43]. Also, in compounds 1–3, C–S vibrations were observed at 825–790, 823–783 and 825–780 cm^{-1}, respectively.

Mass spectral data and major fragments of compounds 1, 2 and 3, along with their molecular complex ion peaks, are given in figures S8–S10. Mass spectral studies showed that the compounds were consistent with their formulation. Molecular ion $[M]^+$ peak was observed for all compounds. Both $[M]^+$ and $[M+H]^+$ were observed for compound 1. The molecular ion mass for the compounds was 309,050 and 310.100 (calculated 309.03) for compound 1, 309,850 (calculated 309.03) for compound 2, and 323.205 (calculated 323.05) for compound 3.

^{1}H-NMR spectra of compounds 1, 2 and 3 are given in figures S2, S4 and S6. Two different OH proton signals were observed for compound 3, while three different OH proton signals were observed for compounds 1 and 2. In compounds 1 and 2, the third hydroxyl protons were found in the form of a single-broad signal. The H-C=N- protons give a singlet for compounds 1–3. The ^{1}H-NMR data for compounds 1–3 show that the tautomeric equilibrium favors the enol-imine form in DMSO. Aromatic protons were observed between 7.04–6.32 ppm for 1–3. Ar-O$\underline{CH_3}$ protons were observed at 3.85 ppm for 3. Ar-SO_2-O$\underline{H}$ protons were observed as a single-broad signal between 3.90–4.10 ppm for compounds 1–3.

In the ^{13}C-NMR spectra of compounds 1–3; there are 13 signals for compounds 1 and 2, and 14 signals for compound 3 (figures S3, S5 and S7). Of all compounds, the imine carbon (–$\underline{C}$=N–) has the highest chemical shift. The methoxy (O$\underline{C}H_3$) carbon in compound 3 has the lowest chemical shift.

UV–vis spectra of the compounds are given in figure 1. If absorption above 400 nm is observed in 2-hydroxy Schiff bases, it is attributed to the Schiff base exhibiting phenyl-amine-keto-amine tautomerism [44]. No signal was observed above 400 nm in DMSO for compounds. This indicates that the compounds are in the phenol-imine form in DMSO. In the UV-Vis spectra of compounds 1 and 2, three bands were observed at 260, 302, 367 nm and 255, 279, 312 nm, while two bands were observed for compound 3 at 267 and 342 nm. These bands

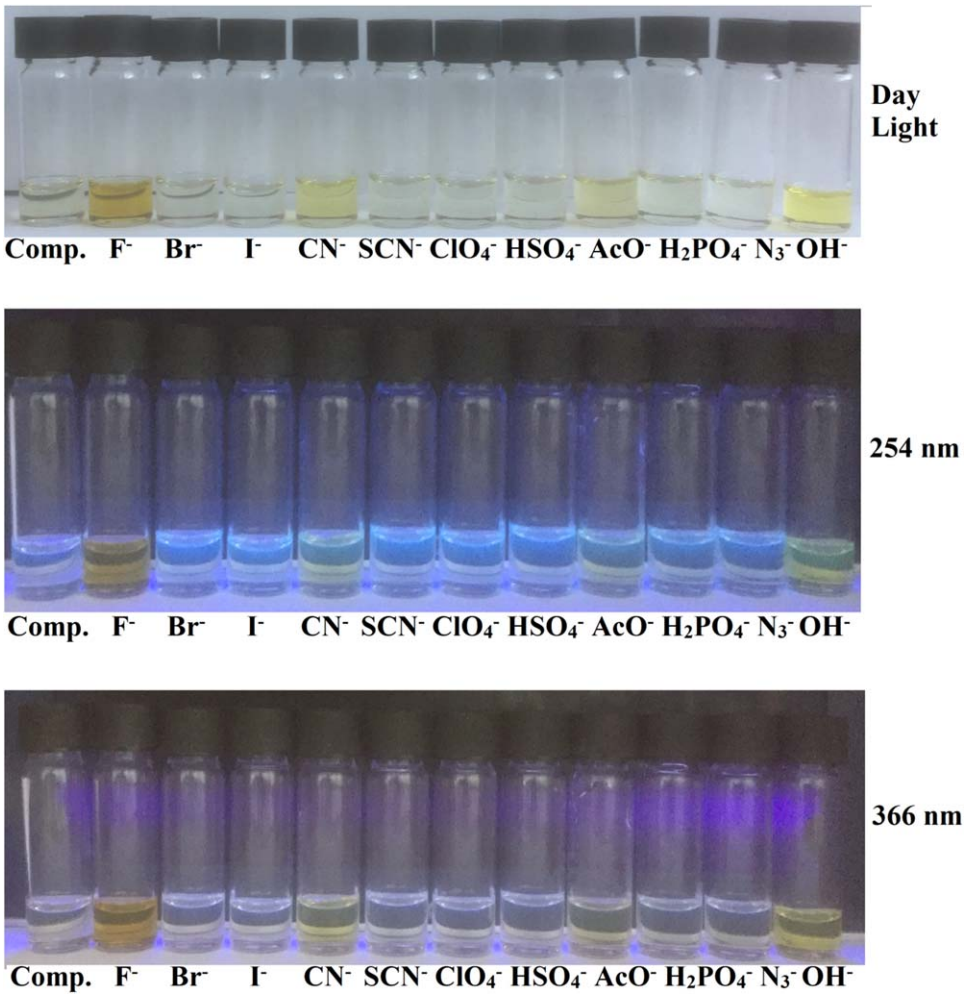


Figure 2. The color changes of compound 1 (1equiv) upon the addition of various anions (3 equiv) of the compound under daylight, and UV lamp ($\lambda = 254$ nm and 366 nm).

are assigned to π–π^* transitions of higher energy C=C, and n–π^* transitions of lower energy C=N and S=O, respectively.

3.2. Colorimetric anion-sensing

The colorimetric detection capability is based on the rapid color change in the solution as soon as ions drop into the receptor Schiff base solution. The colorimetric detection ability of compounds 1–3 were studied in DMSO (figures 2–4). Examining figures 2, 3 and 4, compounds 2 and 3 showed a color change for the F^-, CN^-, AcO^-, $H_2PO_4^-$ and OH^- anions under daylight. However, compound 1 showed a color change for the F^-, CN^-, AcO^- and OH^-, but not for the $H_2PO_4^-$ anion. Compounds 1 and 3 changed from colorless to orange and yellow with the addition of anions under daylight. Compound 2 changes from yellow to orange and pale orange. In daylight, a rapid color change was observed with the addition of anions to the receptor Schiff bases, indicating that these compounds may serve as 'naked-eye' indicators in DMSO for fluoride, cyanide, acetate, dihydrogenphosphate, and hydroxyl ions. Compound 3 showed different color change for anions in both shortwave-UV and longwave-UV. In shortwave-UV there was a discernible fluorescence change to greenish-orange for F^-, and green for CN^-, AcO^-, $H_2PO_4^-$ and OH^- (figure 4). As a result, compound 3 shows fluorescent selectivity for F^-, CN^-, AcO^-, $H_2PO_4^-$ and OH^- in DMSO at both 254 and 366 nm. It can be said that the reason for this is that the OCH_3 group cannot provide enough electrons to the ring and the electron density of the C=N bond decreases.

The anion selectivity of Schiff base receptors was examined by UV–vis spectroscopy (figures S11–S13). Compounds (1–3) and tetrabutylammonium salt solutions were prepared in DMSO. No absorption above 400 nm was observed in the UV–vis spectra in DMSO at room temperature for each compound (figure 1). Then, each anion solution was added to the solution of each compound (3:1) in the UV tube and their UV absorption spectra were recorded. However, with the addition of some anions, both color change and absorption above 400 nm were observed.

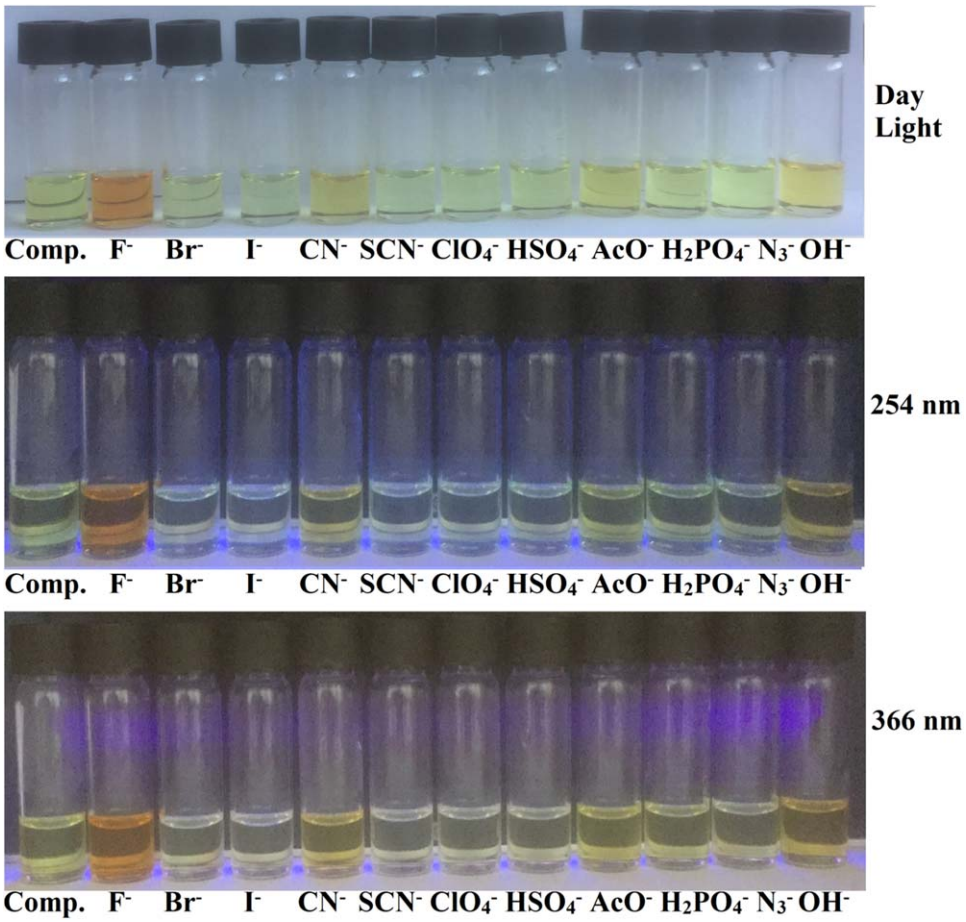


Figure 3. The color changes of compound 2 (1equiv) upon the addition of various anions (3 equiv) of the compound under daylight, and UV lamp ($\lambda = 254$ nm and 366 nm).

Only fluoride, cyanide, acetate, dihydrogenphosphate and hydroxyl anions with the addition of each anion to compounds 2 and 3 gave an absorption band above 400 nm (figures S11–S13). For compound 1, except for $H_2PO_4^-$, absorption was observed for F^-, CN^-, AcO^- and OH^- anions (figure S11). However, neither color change nor absorption was observed for $H_2PO_4^-$ in compound 1 (figures 2 and S11). The colorimetric results for compound 1 are in agreement with the spectroscopic results. No change in absorption was observed with the addition of other iodide, bromide, thiocyanate, perchlorate, hydrogen sulfate, and azide anions to compounds 1, 2 and 3.

3.3. Minimum inhibitory (MIC) and minimum bactericidal concentration (MBC)

The *in vitro* antimicrobial activity spectrums of compounds vary greatly and are presented in table 1. Compound 3 is more active against *C. albicans* 60193 than compounds 1 and 2. However, compounds 1 and 2 show the highest activity against *C. tropicalis* ATCC 13803, while compound 3 is inactive. Again, considering the MIC results, the electron donating of the functional group comes to the fore. Since the OCH_3 group is more electronegative than the OH groups in compounds 1 and 2, the electron density of C=N decreases and *C. tropicalis* ATCC 13803 does not show any counter-effect. However, the compounds (1–3) showed low activity against the tested organisms compared to the reference drugs. Probably because the Schiff bases did not sufficiently penetrate the cells of the microorganisms tested. Compounds 1 and 2 showed the minimum bactericidal concentration (MBC) against *C. tropicalis* ATCC 13803, while compound 3 showed the minimum bactericidal concentration (MBC) against *C. albicans* ATCC 60193.

3.4. DNA-binding

The examination of compound interactions with CT-DNA was performed using UV–vis spectroscopy (figures S14–S16). In the UV–vis spectrum, the presence of hypochromic, hyperchromic, or both effects indicates an interaction with DNA. If the interaction is electrostatic or partially intercalative, hyperchromicity is observed. On the other hand, if the interaction is intercalative, hypochromicity is observed. Additionally, a red or blue shift at the maximum absorption indicates that the compound interacts with DNA [15, 45–48].

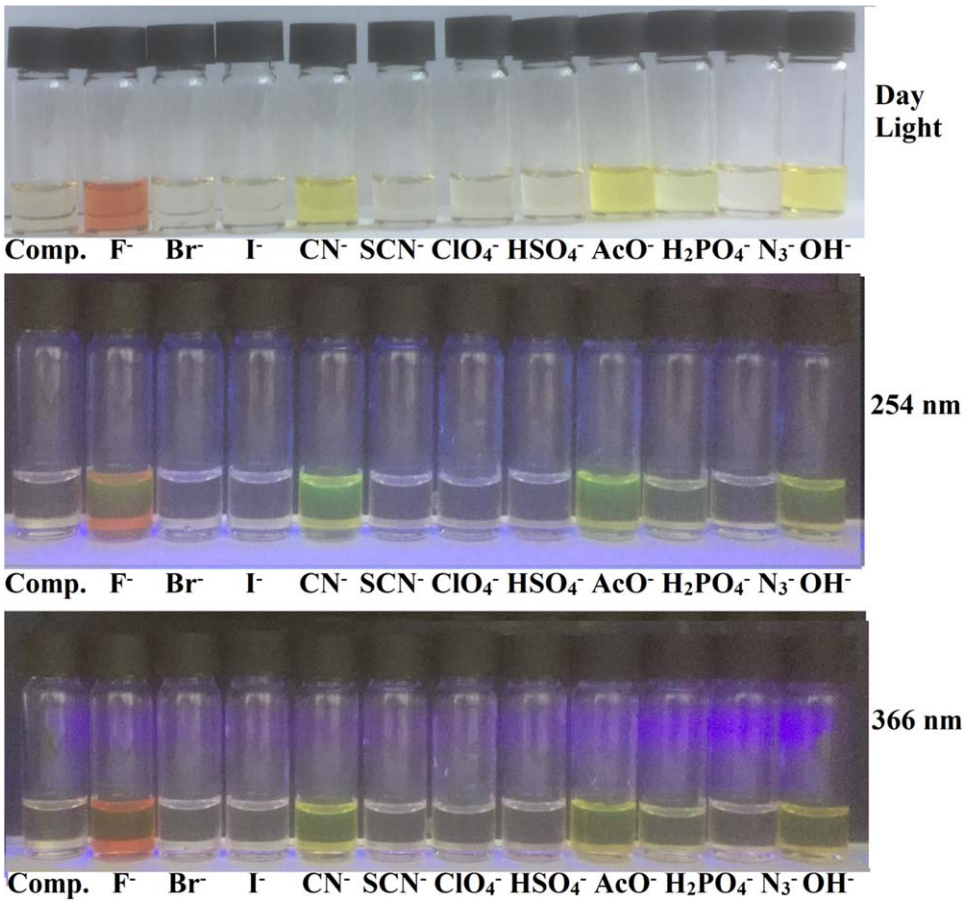


Figure 4. The color changes of compound 3 (1equiv) upon the addition of various anions (3 equiv) of the compound under daylight, and UV lamp ($\lambda = 254$ nm and 366 nm).

We presented the absorption spectra for compounds 1–3 in the absence and presence of CT-DNA in figures S14–S16. The presence of CT-DNA caused an increase in peak intensities in the Schiff base absorption spectra. Aside from a rise in the intensity of the Schiff base bands, the absorption bands of compounds 1, 2, and 3 exhibit a blue shift of 1–4 nm, 1–7 nm, and 1–7 nm, respectively. Blue and red shifts, as well as hyperchromism, are frequently observed to correspond with electrostatic binding strength. As a result, the hyperchromicity effect seen in the absorption spectra suggests that the Schiff bases (1–3) developed an electrostatic mode with DNA.

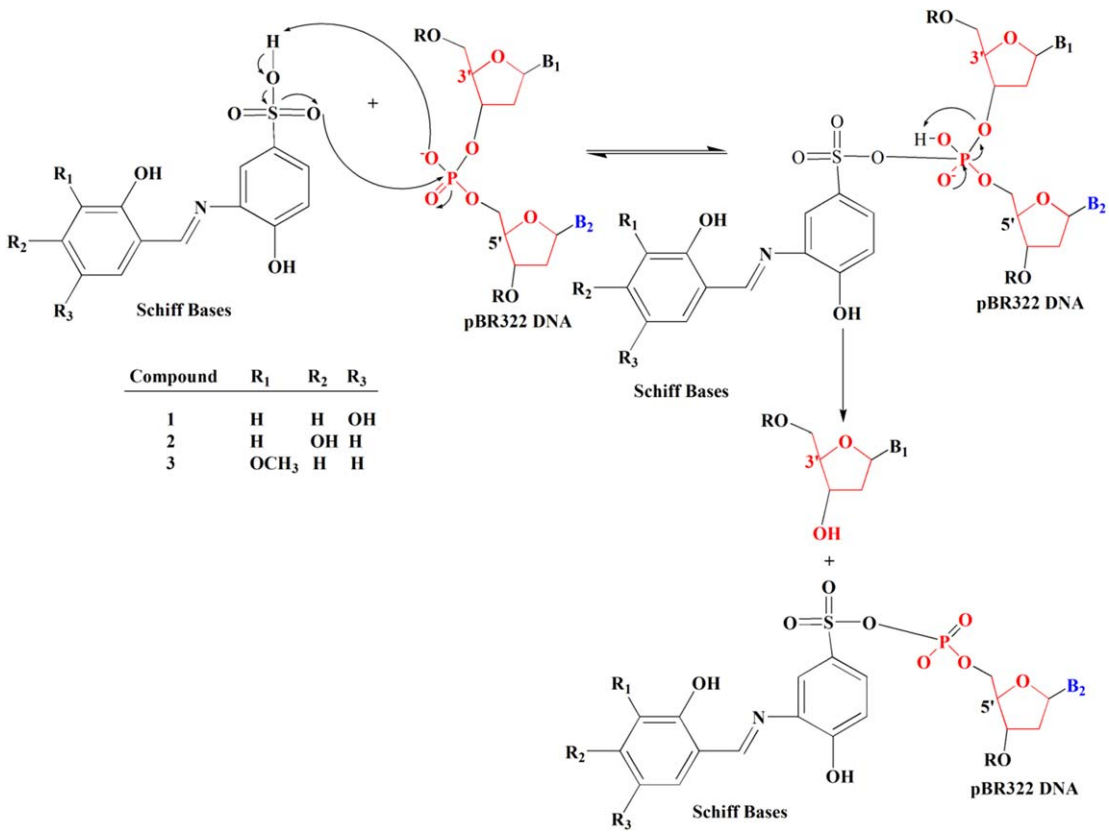
Probably, the proton of the aromaticsulphonic acid is taken up by the phosphate groups of the more basic DNA, forming an anionic Schiff base, and the anionic molecule formed and the protonated DNA interact electrostatically. In addition, the change in the charge distribution of DNA causes its deformation more easily and quickly.

3.5. DNA-cleavage

The most common occurrence in DNA cleavage is the hydrolysis of phosphodiester bonds called hydrolytic cleavage. Secondly, it is oxidative cleavage. Oxidative cleavage occurs when DNA is exposed to oxidative stress or events that lead to the formation of DNA inserts and lesions. Types of oxidative cleavage; glycosidic bond breakage, separation of a nucleobase, and nucleotide excision in which DNA strands are broken.

The DNA cleaving activity of the compounds was examined by gel electrophoresis in the presence of pBR322 DNA. In gel electrophoresis, if a DNA strand break occurs, Form I converts to slower-acting Form II. If both strands are cleaved, a linear Form III occurs between Forms I and II. Cleavage activity results are given in figure S17. All of the compounds cleaved DNA both hydrolytically and oxidatively. The compounds were able to convert the Form I DNA into open circular Form II DNA.

Figure S17 demonstrates that the hydrolytic cleavage activity increases as the concentration of compounds increases. A higher level of cleavage is observed at a concentration of 200 μm. The hydrolytic cleavage mechanism is depicted in Scheme 2. In the hydrolytic cleavage of DNA, the strand break occurs due to the cleavage of the 5'-PO through a nucleophilic attack on the DNA phosphate group 3'-PO. Following this nucleophilic attack, the phosphodiester-sugar 2-deoxyribose bond is severed, resulting in the separation of



Scheme 2. Hydrolytic cleavage mechanism of compounds 1–3.

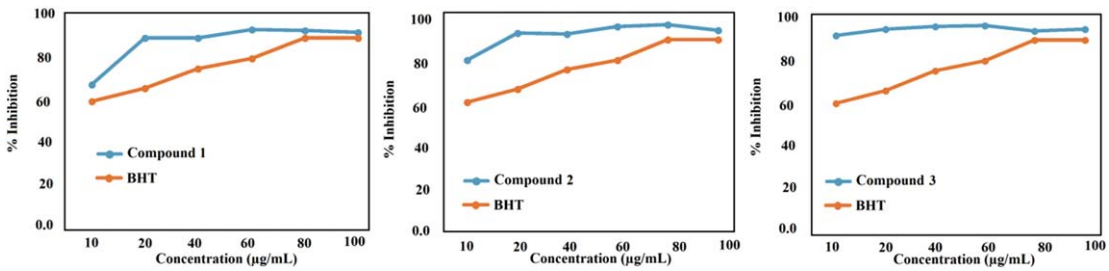


Figure 5. The antioxidant activity of compounds 1–3.

deoxyribose-alcohol. As depicted in figure 2, the first step of the hydrolytic reaction involves the uptake of a proton from the Schiff base sulfonic acid by the DNA phosphate group, leading to the formation of a Schiff base-sulfonate anion. In the second step, the sulfonate anion acts on the phosphorus in the DNA phosphate group, causing the opening of the P=O bond and the formation of a new P-O-SO_2- bond. Finally, the P-O bond quickly closes, and the deoxyribose group, to which the B_1 base is attached, accepts the proton from the phosphate, resulting in the formation of the deoxyribose-alcohol. On the other hand, the oxidative cleavage activity remains unaffected by the concentration of the compounds. The compounds exhibit the same activity at the lowest and highest concentrations.

3.6. Antioxidant activity

The antioxidant activity of the compounds was studied with the DPPH method at concentrations of 10–100 μg ml^{-1}. Antioxidant activities of the compounds (1–3) were 91.27%, 92.77% and 93.66%, respectively, at concentrations of 100 μg ml^{-1} (average of three experiments) (figure 5). Compounds 1, 2 and 3 showed higher activity than standard BHT. Also, when a comparison was made between all three compounds, compound 3 showed higher activities than all of them. This shows that the -OCH_3 group in compound 3 molecule is more electron acceptor. Probably because the OCH_3 group in compound 3 is more electron acceptor, the OH in the

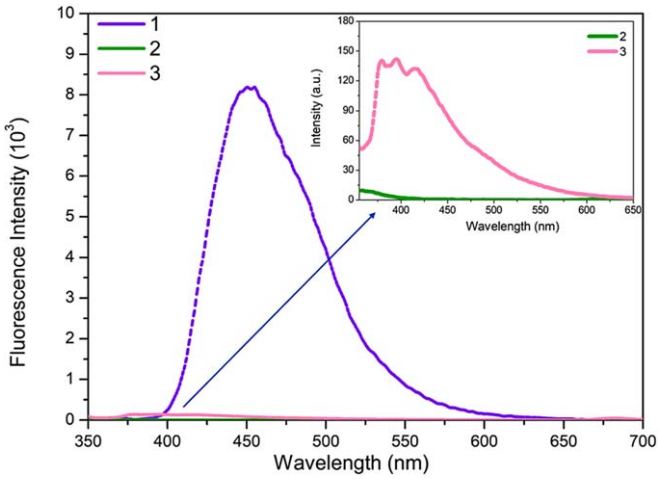


Figure 6. Fluorescence spectra of compounds 1–3 with 5×10^{-5} M in DMSO solution.

molecule can participate in radical reactions more easily. It is possible that Compound 3 can be used as an antioxidant.

3.7. Fluorescence measurements and femtosecond transient absorption spectroscopy studies

The fluorescence spectra of the studied compounds in DMSO solution with 5×10^{-5} M concentration are indicated in figure 6. Compound 1 demonstrated a strong fluorescence signal at a maximum of 450 nm with 367 nm excitation wavelength. Besides, compounds 2 and 3 showed weak fluorescence intensity at a maximum of 353 nm and 395 nm with 295 nm and 340 nm excitation wavelengths, respectively. The reason why the fluorescence is decreased for compound 3 is the less electron donating ability of the methoxy unit. As indicated in figure 6, the position and the strength of the electron-donating moiety dramatically affect the emission properties of the studied compounds.

To obtain a comprehensive understanding of the fluorescence quenching mechanism, charge transfer dynamics, and decay kinetics, femtosecond transient absorption spectroscopy measurements were conducted by dissolving the compounds in a DMSO solution. Based on the linear absorption spectra, the pump wavelength was selected as the maximum absorption wavelength, while the probe wavelength utilized a white light continuum. The transient absorption spectra of the investigated compounds revealed broad positive signals spanning from 420 nm to 840 nm, corresponding to a decrease in singlet excited state absorption (ESA) with increasing time delay, as illustrated in figures 7(a)–c. These ESA signals for the entire set of compounds did not fully decay within the time range of our instrument (3 ns), and the decay traces of these signals are presented in figure 7(d). Notably, compound 2 exhibited a triplet trend, as evidenced by the increasing amplitude of the ESA signal around 440 nm with longer time delays. Consequently, the rates of intersystem crossing (ISC) can be determined by probing the wavelength of 440 nm.

The decay kinetics of the femtosecond transient absorption spectra were fitted using a multiexponential fitting function with the following equation;

$$S(t) = e^{-\left(\frac{t-t_0}{t_p}\right)^2} * \sum_i A_i e^{-\frac{t-t_0}{t_i}},\ t_p = \frac{IRF}{2 \cdot ln2} \quad (1)$$

where t_0 is time zero, A_i and t_i are amplitudes and decay times respectively, IRF is the width of the instrument response function and * is the convolution. The experimental results showed that the Schiff Base incorporated hydroxy group at 2,4 positions demonstrates triplet transition and therefore showed longer excited state lifetime. According to the equation (1), the ISC rate was found at 18 ps for compound 2. On the other hand, compound 3 shows fast charge recombination due to less electron-donating strength of methoxy unit and intramolecular charge transfer as compared to compounds 1 and 2. The less-electron donating property of compound 3 is obviously seen in computational studies.

3.8. Comprehensive analysis of compounds 1–3: optimized molecular structures, solvation, UV–vis, FMOs, MEP, and Hole-Electron Analyses

The crystallographic structure of the investigated compounds could not be determined through X-ray diffraction analysis due to the small crystal sizes. However, it is important to note that experimental validation is crucial for the accuracy and reliability of any computational predictions. While these predicted structures may

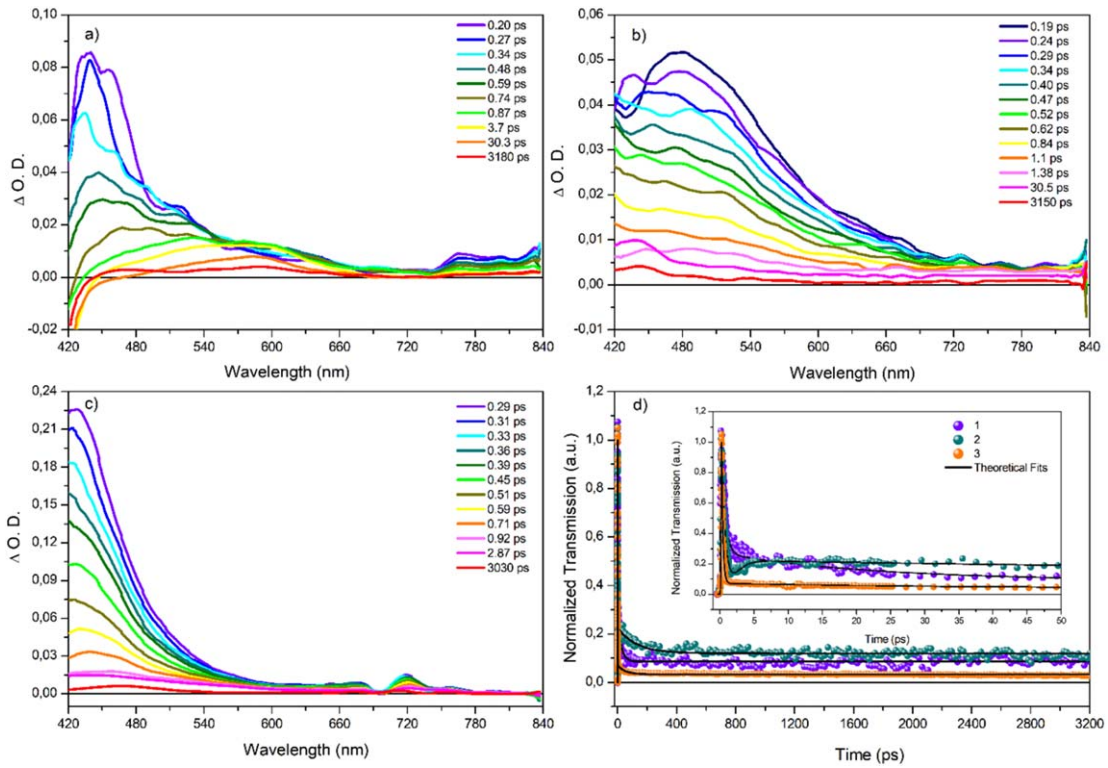


Figure 7. Transient absorption spectra of the compounds (a) 1, (b) 2, (c) 3 with different time delays and (d) decay traces of the compounds 1, 2 and 3 around 430 nm probe wavelength in DMSO solution.

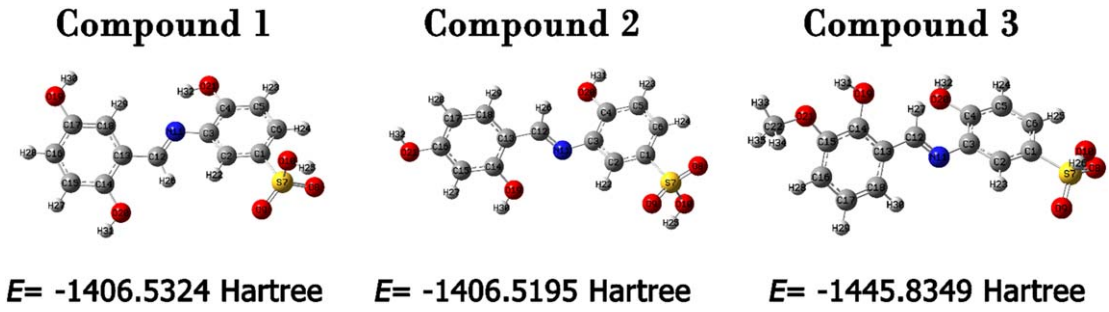


Figure 8. The optimized molecular structures of compounds 1–3.

not be as accurate as experimental results, they can still give valuable insights into the overall molecular properties and behavior. Consequently, we solely relied on theoretical studies to investigate their structural properties. In figure 8, we present a comparison of the optimized structures of the compounds under investigation, while the corresponding geometrical parameters, including bond lengths and angles, are provided in supplementary table S1. The ground state energies refer to the lowest possible energy level that the compound's electrons can occupy for compounds 1 to 3 in their energetically favourable structures. These energies are −1406.5324, 1406.5195, and −1445.8349 Hartree, respectively. From the data presented in table S1, it can be concluded that the calculated geometric parameters are consistent with both the results obtained from theoretical studies and the experimental findings published in the literature [49–51].

In solvation analysis, solvation free energy ($\Delta G_{solvent}$) refers to the energy change associated with the process of dissolving a solute in a solvent. When a solute is introduced into a solvent, interactions occur between the solute particles and the solvent molecules. These interactions can involve various forces such as electrostatic interactions, hydrogen bonding, and van der Waals forces. The solvation free energy takes into account the energetic contributions from the solute-solute interactions, solvent-solvent interactions, and solute-solvent interactions. It represents the overall energy change when a solute molecule transitions from the gas phase (or a less polar medium) to a solution [52, 53].

Table 2. Total energy, solvation energy and dipole moment of compound 1–3 in different solvents.

Solvent	Dielectric constant (ε)	Compound	Total energy (E, hartree)	Solvation energy $\Delta G_{solvent}\left(\frac{kJ}{mol}\right)$	Dipole moment (Debye)
Gas	—	1	−1406.5324	—	4.75
		2	−1406.5195	—	8.52
		3	−1445.8349	—	9.71
Chloroform	4.80	1	−1406.5495	−44.90	6.30
		2	−1406.5408	−55.92	10.74
		3	−1445.8515	−43.38	12.17
Ethanol	24.30	1	−1406.5563	−62.75	9.31
		2	−1406.5490	−77.45	11.55
		3	−1445.8578	−60.12	13.12
DMSO	46.68	1	−1406.5571	−64.85	9.38
		2	−1406.5501	−80.08	11.55
		3	−1445.8586	−62.22	13.25

Mathematically, solvation free energy ($\Delta G_{solvent}$) can be calculated as the difference between the energy of the solute-solvent system ($E_{solvent}$) and the energy of the solute in the gas phase (E_{gas}) [54]: $\Delta G_{solvent} = E_{solvent} - E_{gas}$.

A negative solvation free energy indicates that the solvation process is favorable, meaning the solute tends to dissolve in the solvent. On the other hand, a positive solvation free energy implies an unfavorable process, where the solute is less likely to dissolve. For the investigated compounds, the solvation-free energies were determined in three different common solvents with varying dielectric constants, 4.80 (Chloroform), 24.30 (Ethanol) and 46.68 (DMSO) [53, 55]. The $\Delta G_{solvent}$ values exhibited −44.90 (Chloroform) , −62.75 (Ethanol) and 64.85 kJ mol^{-1} (DMSO) for compound 1, −55.92 (Chloroform) , −77.45 (Ethanol) and −80.08 kJ mol^{-1} (DMSO) for compound 2 and −43.38 (Chloroform) , −60.12 (Ethanol) and 62.22 kJ mol^{-1} (DMSO) for compound 3, as shown in table 2. Consequently, DMSO solvent can be said to be more suitable for solubilizing compound 1–3 due to its high $\Delta G_{solvent}$ value. On the other hand, it can be seen from table 2 that while increasing the dielectric constant, the total energy is decreasing. Increasing the dielectric constant of a medium reduces the strength of electrostatic interactions and enhances solvation effects. Both of these factors contribute to a decrease in the total energy of the system. The dipole moments of compounds 1, 2, and 3 in the gaseous phase are also 4.75, 8.52, and 9.71, respectively. However, when these compounds are in a solution, their dipole moments increase as a result of the long-range interactions between the solvent and the molecules.

A theoretical study of the UV–vis spectra of the investigated compounds was conducted in DMSO solvents, and table 3 summarizes the spectroscopic properties of electronic transitions, including absorption wavelengths, excitation energies, and significant contributions, taking into account the highest oscillator strength [56]. At 359 nm (HOMO → LUMO with 93% contribution), 307 nm (H-1 → LUMO with 85% contribution) and 268 nm (H-4 → LUMO and H-3 → LUMO with 40% and 45% contribution, respectively), we measured the maximum absorbance of compound 1 whose excitation energies are 3.46, 4.03 and 4.63 eV, respectively. The maximum absorbance of compound 2 occurs at 316 nm (HOMO → LUMO with 81% contribution), 275 nm (HOMO → LUMO and H-1 → LUMO with 11% and 65% contribution, respectively), and 255 nm (H-2 → LUMO and HOMO → L+4 with 52% and 14% contribution, respectively) corresponding to excitation energies of 3.92, 4.51 and 4.86 eV respectively. In compound 3, λ_{abs} are detected at 325 nm (HOMO → LUMO and H-1 → LUMO with 65% and 23% contribution, respectively) and 271 nm (H-1 → LUMO, H-2 → LUMO, H-3 → LUMO, H-4 → LUMO with 13%, 44%, 21%, 13% contribution, respectively), with excitation energies of 3.81 and 4.59 eV, respectively. The computational results of UV–Vis absorption spectra are well with the experimental data.

An important factor in assessing chemical reactivity and a molecule's ability to absorb light is the FMOs analysis, also known as HOMOs and LUMOs. The ability of a molecule to be electrophilic (electron-accepting) is determined by LUMO, while its nucleophilic ability (electron-donating) is determined by HOMO. As shown in figure 9, the locations of the red (positive charge) and green lobes (negative charge) on the HOMO-LUMO isosurfaces reveal that the charge density is delocalized on the compound, whereas other locations are localized. We have, however, estimated E_{HOMO}, E_{LUMO}, and the energy difference between HOMO and LUMO (ΔE) which helps determine the optical properties. The values of ΔE are found to be equal to 3.65, 4.32 and 4.13 eV for compounds 1–3, respectively. According to figure 9, compound 1 exhibits a smaller energy gap, indicating that it possesses lower excitation energies for a significant number of its excited states. This implies that compound 1 can be easily activated through photochemical processes. However, the low ΔE also indicates the

Table 3. The maximum absorbance values of electronic transitions for compounds 1–3.

SOLVENT: DMSO COMPOUND	Experimental λ_{abs} (nm)	Theoretical λ_{abs} (nm)	Oscillator strength f	Major contribution	Excitation energy (eV)
	367	359	0.76	HOMO → LUMO (93%)	3.46
1	302	307	0.17	H-1 → LUMO (85%)	4.03
	260	268	0.14	H-4 → LUMO (40%)	4.63
				H-3 → LUMO (45%)	
	312	316	0.75	HOMO → LUMO (81%)	3.92
2	279	275	0.32	HOMO → LUMO (11%)	4.51
				H-1 → LUMO (65%)	
	255	255	0.19	H-2 → LUMO (52%)	4.86
				HOMO → L+4 (14%)	
3	342	325	0.70	HOMO → LUMO (65%)	3.81
				H-1 → LUMO (23%)	
	267	271	0.40	H-1 → LUMO (13%)	4.59
				H-2 → LUMO (44%)	
				H-3 → LUMO (21%)	
				H-4 → LUMO (13%)	

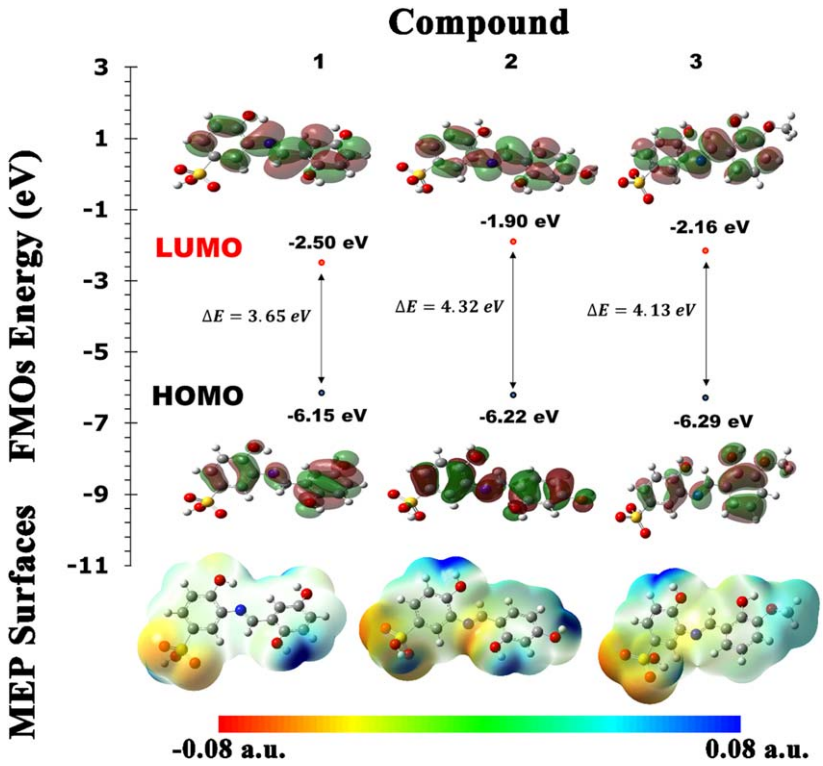


Figure 9. FMOs Energy and MEP surfaces of compounds 1–3.

softness of the molecule, while the high gap between them indicates its hardness [57]. A soft molecule is more reactive and more likely to donate electrons than a hard molecule. The MEP analysis provides an alternative approach for identifying reactive sites susceptible to electrophilic and nucleophilic attacks. Electrophilic reactivity, characterized by negative electrostatic potential, is represented by the red and yellow regions, while nucleophilic reactivity is indicated by the blue region. The green region signifies a zero potential. Examining the MEP surfaces of all compounds in figure 9 reveals distinct patterns: the red regions display high electron density, indicating the presence of electron-withdrawing reactive sites favoring electrophiles, whereas the blue regions exhibit higher positivity, indicating electron-donating reactive sites favoring nucleophiles. It is also useful to investigate and estimate the antioxidant activities of compounds using their MEP isosurfaces. A free radical attack could be privileged in the most positive regions (electron-poor) [58]. Especially in compound 3 as shown in figure 9, the majority of electron-rich surfaces (negative) are located over the SO_3, whereas the electron-poor surfaces (positive) are clustered around the $–OCH_3$ group which is shown in light blue as it donates fewer electrons. It may be possible to use these insights to predict where compound 3 will be attacked by free radicals.

At this stage, it would be valuable to gain further insights into charge transfer (CT) to conduct various analyses within the hole-electron framework for the S_0 (ground state) to S_1 (first excited state) excitation of compounds 1–3. The calculations involve determining several indices, including the *D* parameter (distance between hole and electron centroids), S_r (degree of overlap between hole and electron), *H* (breadth of the average distribution of hole and electron), and *t* (degree of separation between hole and electron). Additionally, the hole delocalization index (*HDI*) and electron delocalization index (*EDI*) [42, 59] are presented in table 4. For $S_0 \rightarrow S_1$ excitation in this study, it can be seen that for all compounds, the *D* indices have very small values (0.69, 0.58 and 0.52 Å, respectively). Next, we examined the S_r index. We found that the S_r indices of all compounds are relatively large (0.71,0 .71 and 0.72 respectively) (the theoretical maximum value is 1.0). We can therefore conclude from the S_r and *D* indices that this excitation is a typical local excitation (LE) for all compounds. Next, we examined the average hole-electron distribution, which is indicated by the *H* index. It can be seen from table 4 that the *H* indices are evidently large (3.09, 2.94 and 2.97, respectively). This means that the distribution of holes and electrons corresponding to the excitations from $S_0 \rightarrow S_1$ are quite wide. One can see that the *t* indices of the $S_0 \rightarrow S_1$ state for all compounds are negative, indicating that their hole and electron are separated to a very low. Therefore, it makes more sense to regard $S_0 \rightarrow S_1$ as an LE. According to the *HDI* and *EDI* indices, hole and electron delocalisation (i.e. uniformity of spatial distribution) is indeed nicely quantified. It can be said that both hole and electron of $S_0 \rightarrow S_1$ excitation are highly delocalized, in agreement with their relatively small *HDI* and *EDI* values.

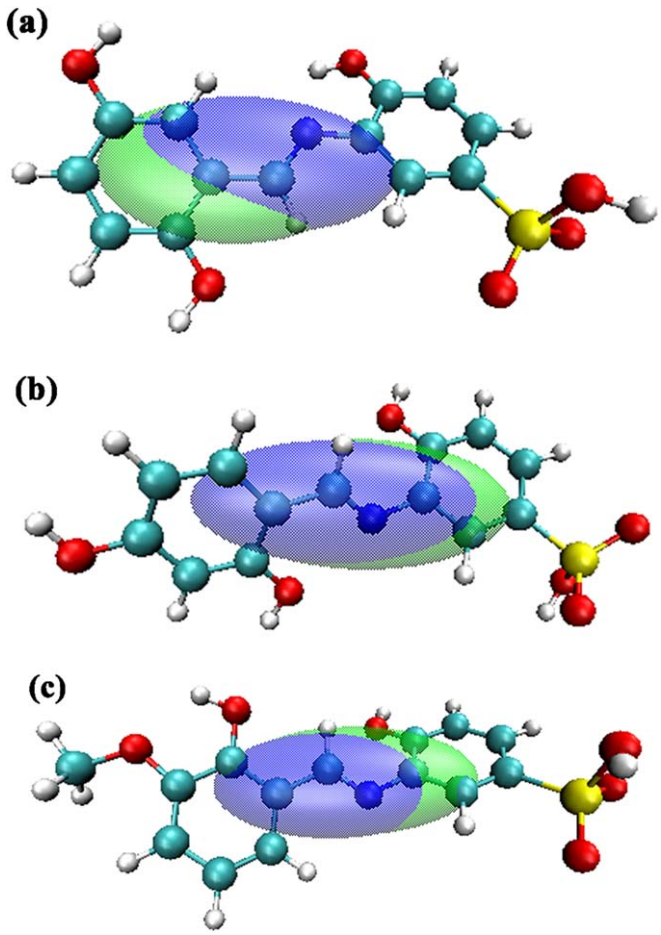


Figure 10. C_{hole}/C_{ele} maps of compounds 1 (a), 2 (b) and 3 (c) for $S_0 \rightarrow S_1$ excitation.

Table 4. The analysis of hole-electron distribution for compounds 1–3 in DMSO solvent.

$S_0 \rightarrow S_1$ excitation state | Compound	1	2	3
D (Å)	0.69	0.58	0.52
S_r	0.71	0.71	0.72
H (Å)	3.09	2.94	2.97
t (Å)	−1.81	−1.79	−1.83
HDI	7.73	9.80	8.79
EDI	7.43	8.19	7.83

A visual representation of a C_{hole}/C_{ele} map is often an effective method, enabling a clearer understanding of charge transfer (CT) or local excitation (LE). These two phenomena have significant implications in diverse processes like photochemical reactions, light absorption, and energy transfer. The occurrence of CT or LE is contingent upon the molecular structure, electronic configuration, and environmental factors specific to the system being investigated. It is clear from figure 10 that the centers of the electron (blue) and hole (green) isosurfaces (namely centroids of C_{hole} and C_{ele}) are close to each other, so they should be viewed as LE functions.

4. Conclusion

In this study, we successfully synthesized imines derived from 3-amino-4-hydroxybenzenesulfonic acid and determined their structures using spectroscopic methods. To further investigate their properties, we employed various spectroscopic techniques, including steady-state absorption, emission, and ultrafast pump-probe

spectroscopy. The UV–vis results obtained from our analysis showed excellent agreement with experimental data, validating the accuracy of our theoretical models. Notably, compound 1 exhibited lower stability but higher chemical reactivity, characterized by a smaller HOMO-LUMO energy gap, making it more susceptible to photochemical excitation. Moreover, compounds 1–3 demonstrated promising potential as chemosensors for anions in DMSO, providing a visible indication to the naked eye under daylight conditions. Among them, compound 3 exhibited selective fluorescence at both 254 and 366 nm. Additionally, our findings revealed that the 3-amino-4-hydroxybenzenesulfonic acid-imines interacted with DNA primarily through an electrostatic mode. Furthermore, compounds 1–3 displayed enhanced antioxidant activity compared to BHT, a commonly used antioxidant compound, and this activity remained stable with increasing concentration. Notably, compound 3 exhibited the highest antioxidant activity among the tested compounds, suggesting its potential application as an effective antioxidant agent. However, fluorescence measurements indicated that the emission signals were significantly influenced by the position and strength of the electron-donating component. Specifically, the addition of a hydroxy or methoxy moiety in proximity to the -OH on the phenyl ring led to a decrease in the fluorescence signal. This decrement in fluorescence signal can be attributed to different mechanisms such as intersystem crossing (ISC) and intramolecular charge transfer, depending on the location of the hydroxy group and the presence of methoxy moieties, respectively. These conclusions were drawn from measurements performed using femtosecond transient absorption spectroscopy. Furthermore, the isosurfaces of C_{hole} and C_{ele} maps indicated that the centroids of all compounds were in close proximity, suggesting that they should be considered as LE (local excitation) functions.

In summary, our study highlights the importance of substituents present in imines derived from 3-amino-4-hydroxybenzenesulfonic acid in determining their biological activities, as well as their impact on optical and sensor characteristics. These findings contribute to a better understanding of the structure-property relationships of these compounds, paving the way for their potential applications in various fields.

Data availability statement

All data that support the findings of this study are included within the article (and any supplementary files).

Declaration of competing interest

The authors declare that they have no known competing financial interests or personal relationships that could have appeared to influence the work reported in this study.

ORCID iDs

Elif Akhuseyin Yildiz https://orcid.org/0000-0001-6485-4660
Yasemin Pepe https://orcid.org/0000-0002-5384-2039
Ahmet Karatay https://orcid.org/0000-0001-9373-801X

References

[1] Zhang Z, Song Q, Jin Y, Feng Y, Li J and Zhang K 2023 *Metals* **13** 386
[2] Fabbrizzi L 2020 *The Journal of Organic Chemistry* **85** 12212–26
[3] Prakash A and Adhikari D 2011 *Int. J. Chem. Tech. Res* **3** 1891–6
[4] Shivhare R, Danao K, Nandurkar D, Rokde V, Ingole A, Warokar A and Mahajan U 2023 Schiff Base as Multifaceted Bioactive Core *Schiff Base in Organic, Inorganic and Physical Chemistry* (Japan: Intechopen) 978-1-80355-679-6 (https://doi.org/10.5772/intechopen.104134)
[5] Al Zoubi W 2013 *International Journal of Organic Chemistry* **2013**
[6] Brkić D R, Božić A R, Marinković A D, Milčić M K, Prlainović N Ž, Assaleh F H, Cvijetić I N, Nikolić J B and Drmanić S Ž 2018 *Spectrochim. Acta, Part A* **196** 16–30
[7] Ebrahimi H P, Hadi J S, Almayah A A, Bolandnazar Z, Swadi A G and Ebrahimi A 2016 *Bioorgan Med. Chem.* **24** 1121–31
[8] Jarrahpour A, Khalili D, De Clercq E, Salmi C and Brunel J M 2007 *Molecules* **12** 1720–30
[9] Bagihalli G B, Avaji P G, Patil S A and Badami P S 2008 *Eur. J. Med. Chem.* **43** 2639–49
[10] Iacopetta D, Ceramella J, Catalano A, Saturnino C, Bonomo M G, Franchini C and Sinicropi M S 2021 *Applied Sciences* **11** 1877
[11] Li L-J, Wang C, Tian C, Yang X-Y, Hua X-X and Du J-L 2013 *Res. Chem. Intermed.* **39** 733–46
[12] Murtaza S, Akhtar M S, Kanwal F, Abbas A, Ashiq S and Shamim S 2017 *Journal of Saudi Chemical Society* **21** S359–72
[13] Alam M S, Choi J-H and Lee D-U 2012 *Bioorgan Med. Chem.* **20** 4103–8
[14] Sriram D, Yogeeswari P, Myneedu N S and Saraswat V 2006 *Bioorganic & medicinal chemistry letters* **16** 2127–9
[15] Ünver H, Boyacıoğlu B, Zeyrek C T, Yıldız M, Demir N, Yıldırım N, Karaosmanoğlu O, Sivas H and Elmalı A 2016 *J. Mol. Struct.* **1125** 162–76
[16] Andiappan K, Sanmugam A, Deivanayagam E, Karuppasamy K, Kim H-S and Vikraman D 2018 *Sci. Rep.* **8** 1–12

[17] Abu-Dief A M and Mohamed I M 2015 *Beni-Suef University Journal of Basic and Applied Sciences* **4** 119–33
[18] Almansour A I, Arumugam N, Prasad S, Kumar R S, Alsalhi M S, Alkaltham M F and Al-Tamimi H b A 2021 *Molecules* **27** 145
[19] Hoffmann R C, Sanctis S and Schneider J J 2017 *Inorg. Chem.* **56** 7550–7
[20] Li Z-Y, Su H-K, Zhou K, Yang B-Z, Xiao T, Sun X-Q, Jiang J and Wang L 2018 *Dyes Pigm.* **149** 921–6
[21] Roy S, Mondal T K, Layek A, Saha R and Sinha C 2018 *Inorg. Chim. Acta* **469** 523–35
[22] Barwiolek M, Sawicka J, Babinska M, Wojtczak A, Surdykowski A, Szczesny R and Szlyk E 2017 *Polyhedron* **135** 153–60
[23] Udhayakumari D and Inbaraj V 2020 *Journal of Fluorescence* **30** 1203–23
[24] Berhanu A L, Mohiuddin I, Malik A K, Aulakh J S, Kumar V and Kim K-H 2019 *Trac-Trend Anal Chem* **116** 74–91
[25] Wang J, Meng Q, Yang Y, Zhong S, Zhang R, Fang Y, Gao Y and Cui X 2022 *ACS Sens.* **7** 2521–36
[26] Goshisht M K, Patra G K and Tripathi N 2022 *Materials Advances* **3** 2612–69
[27] Al Zoubi W and Al Mohanna N 2014 *Spectrochim. Acta, Part A* **132** 854–70
[28] Yildiz E A, Erdener D, Tekin S, Karatay A, Boyacioglu B, Ünver H, Yıldız M and Elmalı A 2022 *J. Photoch Photobio A* **433** 114188
[29] Yildiz E A, Tekin S, Erdener D, Karatay A, Boyacioglu B, Ünver H, Yıldız M and Elmali A 2022 *J. Lumin.* **247** 118849
[30] Tekin S, Karatay A, Erdener D, Yildiz E A, Boyacioglu B, Ünver H, Yıldız M and Elmalı A 2021 *J. Mol. Struct.* **1253** 132239
[31] Yapar G, Demir N, Kiraz A, Özkat G Y and Yıldız M 2022 *J. Mol. Struct.* **1266** 133530
[32] Tysoe S A, Morgan R J, Baker A D and Strekas T C 1993 *J. Phys. Chem.* **97** 1707–11
[33] Kedare S B, Singh R and Food J 2011 *Sci. Tech. Mys.* **48** 412–22
[34] Yehye W A, Rahman N A, Ariffin A, Abd Hamid S B, Alhadi A A, Kadir F A and Yaeghoobi M 2015 *Eur. J. Med. Chem.* **101** 295–312
[35] DenningtonR, KeithT and MillamJ (2009) Gauss View Version 5. Semichem Inc. Shawnee Mission.
[36] Becke A *Chem. Phys.* **98** 5648
[37] Lee C, Yang W and Parr R G 1988 *Physical review B* **37** 785
[38] Frisch M, Trucks G, Schlegel H B, Scuseria G E, Robb M A, Cheeseman J R, Scalmani G, Barone V, Mennucci B and Petersson G 2009 *Inc., Wallingford CT* **201**
[39] Jadoon T, Mahmood T, Ayub K and Phys J 2021 *Chem. Solids* **153** 110028
[40] Mombrú D, Romero M, Faccio R and Mombrú Á W 2019 *Physica E: Low-dimensional Systems and Nanostructures* **113** 130–6
[41] Feng J, Guo Q, Song N, Liu H, Dong H, Chen Y, Yu L and Dong L 2021 *Diam. Relat. Mater.* **113** 108264
[42] Lu T and Chen F 2012 *J. Comput. Chem.* **33** 580–92
[43] Chohan Z H, Shad H A, Supuran C T and Enzym J 2012 *Inhib Med. Ch.* **27** 58–68
[44] Nazır H, Yıldız M, Yılmaz H, Tahir M and Ülkü D 2000 *Journal of Molecular Structure 524* 241–50
[45] Yıldız M, Karpuz Ö, Zeyrek C T, Boyacıoğlu B, Dal H, Demir N, Yıldırım N and Ünver H 2015 *J. Mol. Struct.* **1094** 148–60
[46] Barare B, Yıldız M, Alpaslan G, Dilek N, Ünver H, Tadesse S and Aslan K 2015 *Sensors Actuators B* **215** 52–61
[47] Barare B, Yıldız M, Ünver H and Aslan K 2016 *Tetrahedron Lett.* **57** 537–42
[48] Zeyrek C T, Boyacioğlu B, Yıldız M, Ünver H, Yolal D, Demir N, Elmali A, Tadesse S and Aslan K 2016 *Bioorgan Med. Chem.* **24** 5592–601
[49] Noureddine O, Gatfaoui S, Brandán S A, Marouani H and Issaoui N 2020 *J. Mol. Struct.* **1202** 127351
[50] Romani D, Tonello I S and Brandán S A 2016 *Heliyon* **2** e00190
[51] Chahar F C, Alvarez P E, Zampini C, Isla M I and Brandán S A 2020 *J. Mol. Struct.* **1201** 127221
[52] Duarte Ramos Matos G, Kyu D Y, Loeffler H H, Chodera J D, Shirts M R and Mobley D L 2017 *Journal of Chemical & Engineering Data* **62** 1559–69
[53] Al-Otaibi J S, Ullah Z, Mary Y S, Mary Y S, Soman S, Thirunavukkarasu M and Kwon H W 2022 *Vietnam Journal of Chemistry* **60** 636–52
[54] Parsa P, Ghiasi R and Marjani A 2021 *Inorg. Chem. Commun.* **127** 108497
[55] Marenich A V, Cramer C J and Truhlar D G 2009 *J. Phys. Chem. B* **113** 6378–96
[56] Ruger R, Van Lenthe E, Lu Y, Frenzel J, Heine T and Visscher L 2015 *J. Chem. Theory Comput.* **11** 157–67
[57] Koopmans T 1933 *Physica* **1** 104–13
[58] Boulebd H 2020 *Free Radical Res.* **54** 221–30
[59] Liu Z, Lu T and Chen Q 2020 *Carbon* **165** 468–75